minerals

MDPI

Article

Amgaite, $Tl^{3+}{}_2Te^{6+}O_6$, a New Mineral from the Khokhoyskoe Gold Deposit, Eastern Siberia, Russia

Anatoly V. Kasatkin [1], Galina S. Anisimova [2], Fabrizio Nestola [3,*], Jakub Plášil [4], Jiří Sejkora [5], Radek Škoda [6], Evgeniy P. Sokolov [7], Larisa A. Kondratieva [2] and Veronika N. Kardashevskaia [2]

1 Fersman Mineralogical Museum of Russian Academy of Sciences, 119071 Moscow, Russia
2 Diamond and Precious Metal Geology Institute, Siberian Branch, Russian Academy of Sciences, Prospekt Lenina, 39, 677000 Yakutsk, Russia
3 Dipartimento di Geoscienze, Università di Padova, Via Gradenigo 6, I-35131 Padova, Italy
4 Institute of Physics ASCR, v.v.i., Na Slovance 1999/2, 182 21 Prague, Czech Republic
5 Department of Mineralogy and Petrology, National Museum, 193 00 Prague, Czech Republic
6 Department of Geological Sciences, Faculty of Science, Masaryk University, Kotlářská 2, 611 37 Brno, Czech Republic
7 Russian Geological Survey "Yakutskgeologiya", Kalvitsa ul. 24, 677009 Yakutsk, Russia
* Correspondence: fabrizio.nestola@unipd.it; Tel.: +39-39-26755113

Abstract: The new mineral amgaite was discovered at the Khokhoyskoe gold deposit, 120 km W of Aldan town, Aldanskiy District, Sakha Republic (Yakutia), Eastern Siberia, Russia. Amgaite forms fine-grained colloform aggregates up to 0.05 mm across, and is often intimately intergrown with avicennite, unidentified carbonates and antimonates of Tl. Other associated minerals include gold, silver, acanthite, arsenopyrite, pyrite, berthierite, chalcocite, weissbergite, chlorargyrite, calcite, quartz, goethite etc. Amgaite is dark reddish brown to black. It has submetallic luster, black streak, brittle tenacity and conchoidal fracture. Its density calculated from the empirical formula and powder XRD data is 8.358 g/cm^3. Its Mohs' hardness is ca. 1.5–2. Optically, amgaite is uniaxial. In reflected light, it is gray with a bluish shade, very weakly anisotropic with rare brownish red internal reflections. Reflectance values for the four COM wavelengths [R_{min}, R_{max} (%)(λ in nm)] are: 13.5, 14.2 (470); 12.7, 13.2 (546); 12.3, 12.7 (589); and 11.7, 12.3 (650). The Raman spectrum shows bands of Te–O and Tl–O bonds and confirms the absence in amgaite of H_2O, OH^-, CO_3^{2-} groups and B–O bonds. The chemical composition is (electron microprobe, wt.%): MgO 0.43, CaO 1.62, Fe_2O_3 0.36, Tl_2O_3 66.27, Sb_2O_5 3.48, TeO_3 27.31, total 99.47. The empirical formula based on 6 O *apfu* is $Tl^{3+}{}_{1.74}Ca_{0.17}Mg_{0.06}Fe^{3+}{}_{0.03}Te^{6+}{}_{0.93}Sb^{5+}{}_{0.13}O_6$. Amgaite is trigonal, space group *P*321; unit-cell parameters are as follows: a = 9.0600(9), c = 4.9913(11) Å, V = 354.82(8) Å^3, Z = 3. The strongest lines of the powder X-ray diffraction pattern [d_{obs}, Å (I, %) (hkl)] are as follows: 3.352 (100) (111), 3.063 (15) (201), 2.619 (49) (300), 2.065 (18) (221), 1.804 (28) (302), 1.697 (8) (321), 1.625 (9) (411). The crystal structure of amgaite is the same as of synthetic $Tl^{3+}{}_2Te^{6+}O_6$. The new mineral is named after the Amga River, the basin of which hosts the type locality, Khokhoyskoe occurrence. The type material is deposited in the collections of the Fersman Mineralogical Museum of the Russian Academy of Sciences, Moscow, Russia, with the registration number 5773/1.

Keywords: amgaite; new mineral; Khokhoyskoe gold deposit; Amga river; Raman spectroscopy; chemistry; synthetic $Tl^{3+}{}_2Te^{6+}O_6$; trivalent thallium

Citation: Kasatkin, A.V.; Anisimova, G.S.; Nestola, F.; Plášil, J.; Sejkora, J.; Škoda, R.; Sokolov, E.P.; Kondratieva, L.A.; Kardashevskaia, V.N. Amgaite, $Tl^{3+}{}_2Te^{6+}O_6$, a New Mineral from the Khokhoyskoe Gold Deposit, Eastern Siberia, Russia. *Minerals* **2022**, *12*, 1064. https://doi.org/10.3390/min12091064

Academic Editors: Pei Ni, Mincheng Xu, Tiangang Wang, Junyi Pan and Yitao Cai

Received: 30 July 2022
Accepted: 22 August 2022
Published: 24 August 2022

1. Introduction

Thallium and its compounds are consumed in a wide variety of industrial applications, such as high-temperature superconducting materials, gamma and infrared radiation detection and transmission equipment, acoustic-optical measuring devices, photoelectric cells, magnetic resonance imaging, electric power generation and transmission, fabrication of optical lenses with a high refractive index, cardiovascular scintigraphy and diagnosis

of malignant tumors in medicine etc. [1,2]. In mineralogy and gemology, Clerici solution (a mixture of thallium formate and thallium malonate) is used as a liquid to measure the density of minerals and precious stones and for sink-float separation of minerals [3]. On the other side, thallium is considered one of the most toxic heavy metals on Earth and the use of its compounds should be vigorously controlled to prevent harm to humans and the environment [4].

Although thallium is reasonably abundant in the Earth's crust at a concentration estimated to be about 0.7 part per million (ppm), it is mostly disseminated in soils, in associated potassium minerals in clays and granites, in ferromanganese crusts and nodules that cover the surface of seamounts and seafloors throughout the oceans, and is not generally considered to be commercially recoverable from those materials [1,5,6]. The major sources of recoverable thallium are gold and complex sulfide ores. According to [7], thallium contents in common sulfides might reach up to 3200 ppm. In view of the above, much attention of geologists and mineralogists is given to the research of gold deposits that bear Tl-mineralization and the study of new Tl-bearing mineral species and their structures [8–10].

In the present paper, we provide a description of a new mineral species with the formula $Tl^{3+}{}_2Te^{6+}O_6$, which was discovered at the Khokhoyskoe gold deposit in Eastern Siberia in the Russian Federation. This new species was named amgaite [pronounced: əm gay ait; Russian Cyrillic-амгаит] after the Amga River, the basin of which hosts the type locality, Khokhoyskoe gold deposit.

The mineral, its name and mineral symbol (Amgt) have been approved by the IMA Commission on New Minerals, Nomenclature and Classification (CNMNC) with the number 2021–104 [11]. The holotype material is deposited in the collections of the Fersman Mineralogical Museum of the Russian Academy of Sciences, Moscow, Russia, with the registration number 5773/1.

2. Occurrence, Geological Settings and Mineral Association

The new mineral was found in a heavy concentrate obtained by hydroseparation from friable clayey-sandy material collected in the summer of 2015 by one of the authors (E.P.S.) at the Khokhoyskoe (Khokhoy) gold deposit located 120 km W of Aldan town, in the upstream of Khokhoy creek, a right tributary of the Amga River, in the Aldanskiy region of Sakha Republic (Yakutia), Eastern Siberia, Russia (59°06′36″ N, 123°14′42″ E) (Figure 1). The routine SEM/EDS inspection of polished sections with the above heavy concentrate revealed a number of unidentified antimonates, carbonates and tellurates of thallium [12,13], including the new mineral described herein.

(**a**) (**b**)

Figure 1. Khokhoyskoe gold deposit, summer 2017: (**a**) exploration trench, (**b**) the place where material with amgaite was sampled. Photo: Larisa A. Kondratieva.

The Khokhoyskoe gold deposit is confined to the Khokhoy gold ore field, located in the Verkhneamginskaya auriferous zone. The site is located on the northern slope of the Aldan shield, in the area of subsidence of the basement and increase of the thickness of the sedimentary cover (Figure 2). The main volume of the sediments is represented by Lower Cambrian terrigenous-carbonate deposits with stratigraphic unconformity overlain by Lower Jurassic terrigenous sandstone sediments. Mesozoic magmatism resulted in little stratified intrusions, monzonite lakkolithes and syenite-porphyries, as well as dikes of alkaline gabbroids. The ore field is structured by a vast faulted area with the North-Eastern strike. Mineralization is developed at the nodes of the intersection of feathering faults at the tectonized point of contact of the Cambrian and Jurassic sediments. The ores are concentrated in karst cavities that form an extended zone striking more than 10 km long, crossing the ore field from the South to the North. The width of the karst cavities, exposed by mine workings, ranges from 5 to 50 m, their depth—from 15 to 45 m. Karst cavities are filled with intensely limonitized clayey-sandy brown formations containing multiple fragments of primary ores and host rocks. The main gangue minerals of karst cavities are fine-grained quartz and quartz var. chalcedony, opal, potassic feldspar (adularia), muscovite, illite, calcite and fluorite. Main ore minerals of macroscopic size include baryte, hollandite and oxidized and hematitized pyrite. All other ore minerals form microinclusions. These include acanthite, arsenopyrite, avicennite, berthierite, bismoclite, chalcocite, chlorargyrite, cinnabar, coloradoite, gold, jankovićite, parapierrotite, silver and weissbergite. According to the mineral composition and geochemical signature (Au, Tl, Sb, As, Te, Hg), the Khokhoyskoe gold deposit is comparable to the Kuranakh deposit in Russia and the Carlin-type gold deposits [12–15].

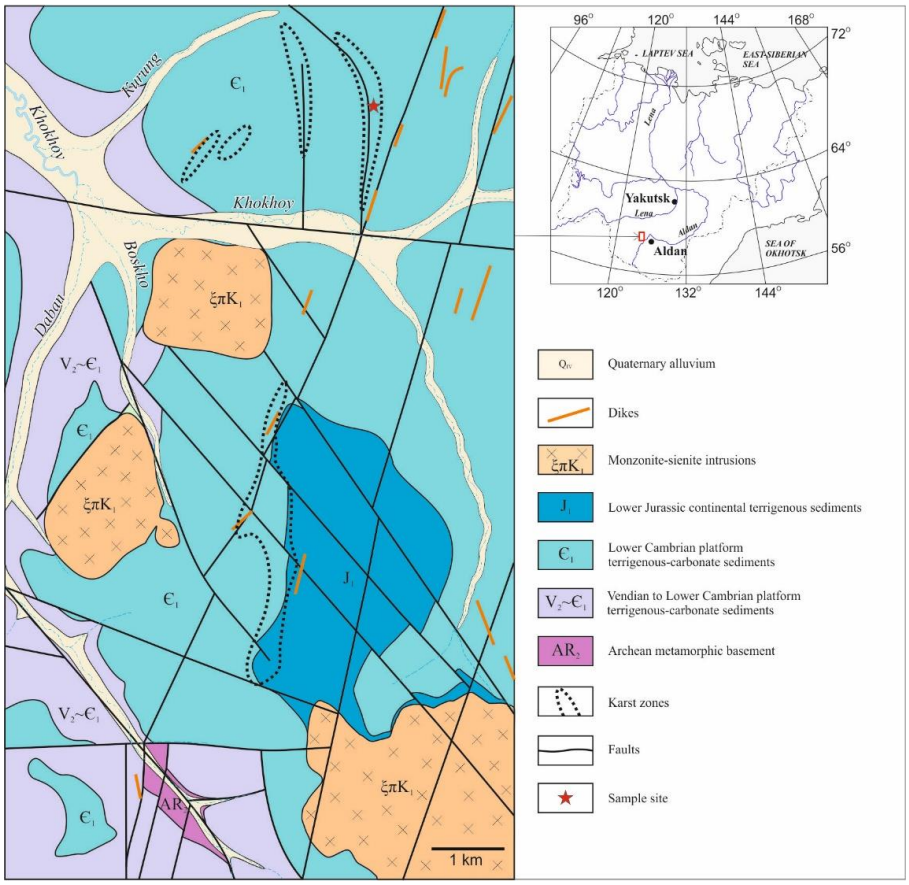

Figure 2. Geographical location and geological position and structure of Khokhoyskoe gold deposit [12].

The gold at the Khokhoyskoe deposit has a supergene origin and is represented by two morphological types. The first type is represented by gold crystals and irregular masses, with fineness ranging from 835% to 1000%. The second type is represented by mustard gold with microporous and dendritic internal structure. Its fineness is above 900% [12,14].

Gold of both types occurs in association with amgaite.

3. General Appearance, Physical, Chemical and Optical Properties

Amgaite occurs as very fine-grained colloform aggregates up to 0.05 mm across; some grains have a botryoidal shape (Figure 3a,b). Amgaite is often intimately intergrown with avicennite and unidentified carbonates and antimonates of Tl. Rarely, it is observed along cracks in gold grains and particles. The new mineral is opaque and has a very dark reddish brown to black color. Its streak is black and its lustre is sub-metallic. It is brittle with a conchoidal fracture. Neither cleavage nor parting are observed. Amgaite is non-fluorescent under ultraviolet light. It is very soft with a hardness estimated at 1.5–2 on Mohs' scale. The density was not measured due to small grain size and intimate intergrowth with avicennite and other phases. However, its density calculated from the empirical formula and unit–cell volume obtained from PXRD data is 8.358 g/cm^3. The new mineral is insoluble in water but dissolves in hot nitric acid.

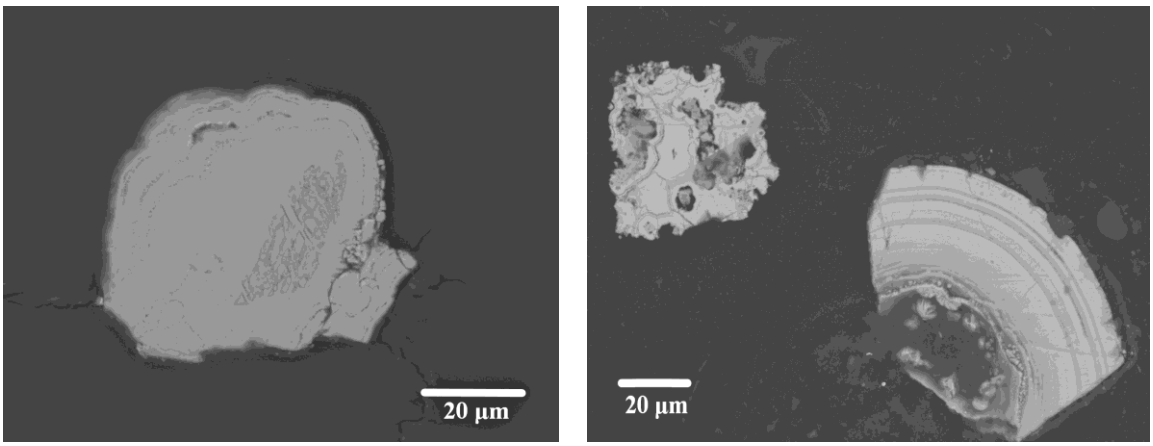

(**a**) (**b**)

Figure 3. Aggregates of amgaite. Polished section. SEM (BSE) images. (**a**) botryoidal aggregate (**b**) fragments of colloform aggregates.

Optically, amgaite is uniaxial. However, its refractive indices could not be measured correctly because of a cryptocrystalline character, the very high birefringence of the grains and their extremely inhomogeneous nature due to numerous inclusions of avicennite and other phases. The Gladstone-Dale relationship predicts an average index of refraction of 1.78. Amgaite's optical properties were studied using the methods common for metallic minerals. In reflected light, amgaite is gray with a bluish shade. No bireflectance or pleochroism are observed. Under crossed polars, it is very weakly anisotropic. Internal reflections are rare, and brownish red in color. Reflectance spectra were collected at the Department of Mineralogy and Petrology, National Museum of Prague, Czech Republic. Reflectance values were measured in air with a TIDAS MSP400 spectrophotometer attached to a Leica microscope (100× objective) using a WTiC (Zeiss no. 370) standard, with a square sample measurement field of ca. 7 × 7 µm. The results from the 400–700 nm range are given in Table 1 and plotted in Figure 4.

Table 1. Reflectance values (%) for amgaite.

R_{max}	R_{min}	λ (nm)	R_{max}	R_{min}	λ (nm)
16.2	15.3	400	13.1	12.6	560
15.7	14.7	420	12.8	12.4	580
15.1	14.2	440	12.7	12.3	589
14.4	13.7	460	12.7	12.2	600
14.2	13.5	470	12.5	12.0	620
14.1	13.4	480	12.4	11.8	640
13.8	13.3	500	12.3	11.7	650
13.5	13.0	520	12.2	11.7	660
13.3	12.8	540	12.2	11.6	680
13.2	12.7	546	12.1	11.6	700

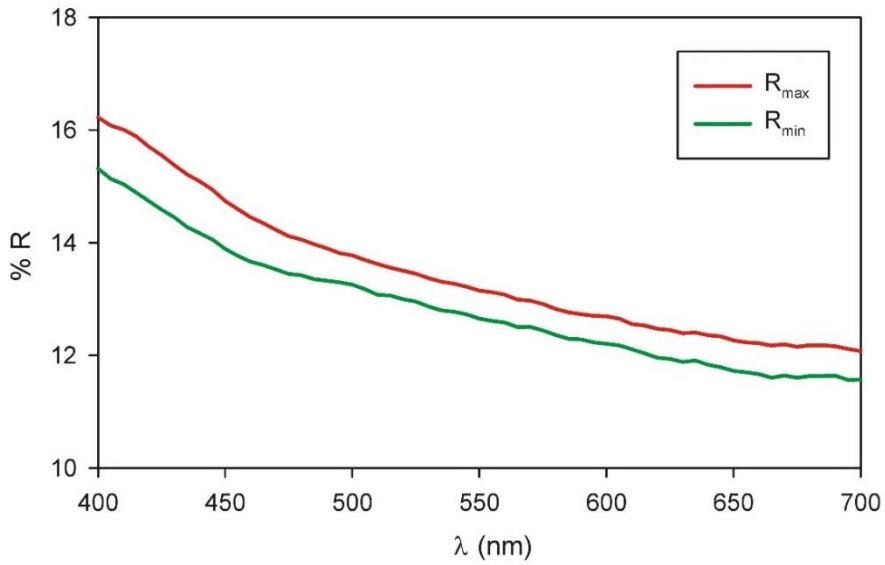

Figure 4. Reflectivity curves for amgaite.

The reference wavelengths required by the commission on Ore Mineralogy (COM) are given in bold.

4. Raman Spectroscopy

The Raman spectra of amgaite (Figure 5) were collected at the Department of Mineralogy and Petrology, National Museum of Prague, Czech Republic, in the range 4000–140 cm^{-1} using a DXR dispersive Raman Spectrometer (Thermo-Scientific, Waltham, MA, USA) mounted on a confocal Olympus microscope. The Raman signal was excited by an unpolarised 633 nm He-Ne gas laser and detected by a CCD detector (size 1650 × 200 pixels, Peltier-cooled to −60 °C, quantum efficiency 50% and dynamic range 360–1100 nm). The experimental parameters were as follows: 100× objective, 10 s exposure time, accumulation of 100 exposures, 50 μm pinhole spectrograph aperture and 2.5 mW laser power level. The spectra were repeatedly acquired from different grains in order to obtain a representative spectrum with the best signal-to-noise ratio. The possible thermal damage of the measured point was excluded and assessed by visual inspection of the exposed surface after measurement, observation of possible decay of spectral features at the start of excitation and checking for thermal downshift of Raman lines. The instrument was set up by a software-controlled calibration procedure using multiple neon emission lines (wavelength calibration), multiple polystyrene Raman bands (laser-frequency calibration) and standardized white-light sources (intensity calibration). Spectral manipulations were performed using the Omnic 9 software (Thermo-Scientific). Gaussian/Lorentzian (pseudo-Voigt) profile functions of the band-shape were used to obtain decomposed band components of the spectra. The decomposition was based on the minimization of the difference in the

observed and calculated profiles until the squared correlation coefficient (r^2) was greater than 0.995.

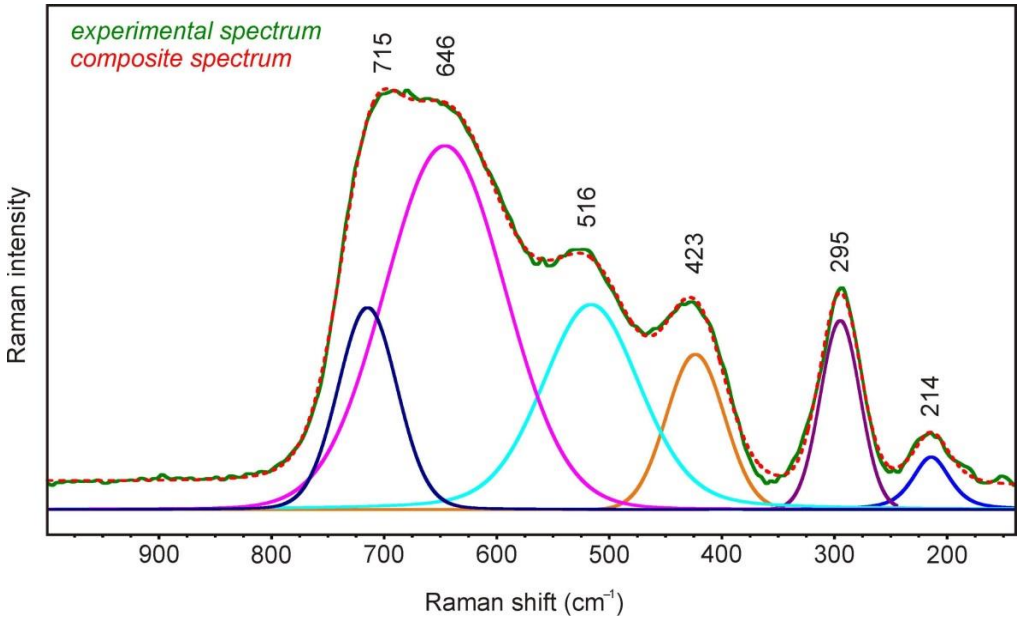

Figure 5. Raman spectrum of amgaite.

An absence of Raman bands in the region above 1000 cm^{-1} confirms the absence of molecular water, $(OH)^-$ and $(CO_3)^{2-}$ groups and B–O bonds in amgaite. The main band in the spectrum consists of two components at 715 and 646 cm^{-1} and exhibits distinct shoulders at 516 and 423 cm^{-1}. The bands in this area are possibly assigned to ν_1, ν_2 and ν_5 vibrations of Te–O bonds in the TeO_6 octahedra [16–18]. The bands at 295 and 214 cm^{-1} may be connected to vibrations of Tl–O bonds; bands with maxima approximately 310 and 230 cm^{-1} are possible to observe at the spectrum of avicennite Tl_2O_3 (RRUFF R070262.2) [19].

5. Chemical Composition

Chemical analyses (7) were carried out at the Department of Geological Sciences, Faculty of Science of Masaryk University in Brno, Czech Republic with a Cameca SX-100 electron microprobe (WDS mode, 15 kV, 10 nA, 2 μm beam diameter). Analytical data for amgaite are given in Table 2. Contents of other elements with atomic numbers higher than that of beryllium are below detection limits. Raw intensities were processed by X-PHI matrix correction algorithm.

Table 2. Chemical data for amgaite.

Constituent	Wt.%	Range	Standard Deviation	Reference Material
MgO	0.43	0.31–0.53	0.10	pyrope
CaO	1.62	1.50–1.69	0.09	fluorapatite
Mn_2O_3	0.25	0.18–0.35	0.07	rhodonite
Fe_2O_3	0.16	0.13–0.19	0.02	hematite
Tl_2O_3	66.27	64.68–67.12	0.98	Tl(Br, I)
Sb_2O_5	3.48	2.11–5.74	1.51	Sb
TeO_3	27.31	26.10–28.87	0.97	HgTe
Total	99.52			

The empirical formula calculated on the basis of 6 O *apfu* being $Tl^{3+}_{1.74}Ca_{0.17}Mg_{0.06}Mn^{3+}_{0.02}Fe^{3+}_{0.01}Te^{6+}_{0.93}Sb^{5+}_{0.13}O_6$. Due to extremely oxidative conditions at the Khokhoyskoe occurrence, Mn and Fe are assumed to be trivalent, while Sb is considered to have 5+ valence state.

The ideal formula of amgaite is $Tl^{3+}_2Te^{6+}O_6$, which requires Tl_2O_3 72.24, TeO_3 27.76, a total of 100 wt.%.

6. X-ray Diffraction

The single-crystal X-ray diffraction studies could not be carried out because of the absence of single crystals: aggregates of amgaite are cryptocrystalline and inhomogeneous. However, we collected powder micro-X-ray diffraction data (Table 3, Figure 6) using a Rigaku Oxford Diffraction Supernova diffractometer working in micro-powder diffraction transmission mode installed at the Department of Geosciences, University of Padova, Italy. The diffractometer was equipped with a Mo$K\alpha$ X-ray micro-source (conditions: 50 kV, 0.12 mA) and a Pilatus 200K Dectris detector with a detector-to-sample distance equal to 68 mm. The data were collected over 40° around the phi axis with an exposure time of 120 s/°. Due to the low intensity of diffraction data, we were able to detect reflections only between about 3.50 and 1.50 Å.

Table 3. Powder X-ray data (*d* in Å) for amgaite compared with that of the synthetic $Tl^{3+}_2Te^{6+}O_6$ [20].

Amgaite		$I_{obs.}$ [%]	*hkl*	Synthetic $Tl^{3+}_2Te^{6+}O_6$		$I_{calc.}$ [%]
d_{obs}	d_{calc}			d_{obs}	d_{calc}	
3.352	3.354	100	1 1 1	3.36	3.354	100
3.063	3.084	15	2 0 1	3.09	3.085	34
2.619	2.615	49	3 0 0	2.62	2.618	36
2.541	2.550	7	2 1 1	2.55	2.551	12
2.313	2.317	4	3 0 1	2.32	2.318	2
2.189	2.186	2	1 1 2	2.19	2.179	6
2.065	2.063	18	2 2 1	2.06	2.064	13
1.911	1.909	4	2 1 2	1.910	1.909	10
1.804	1.806	28	3 0 2	1.806	1.805	32
1.697	1.693	8	3 2 1	1.695	1.695	17
1.625	1.620	9	4 1 1	1.621	1.621	7
1.506	1.510	7	3 3 0	1.512	1.512	5

The unit–cell parameters were calculated from the observed *d* spacings reported in Table 3 using UNITCELL software [21]. Amgaite is trigonal, from space group *P*321(#150), a = 9.0600(9), c = 4.9913(11) Å, V = 354.82(8) Å^3; Z = 3. These data are in very good agreement with the synthetic $Tl^{3+}_2Te^{6+}O_6$ described by [20]. For comparison, the unit–cell data of the synthetic analogue are: a = 9.070, c = 4.984 Å, V = 355.1 Å^3.

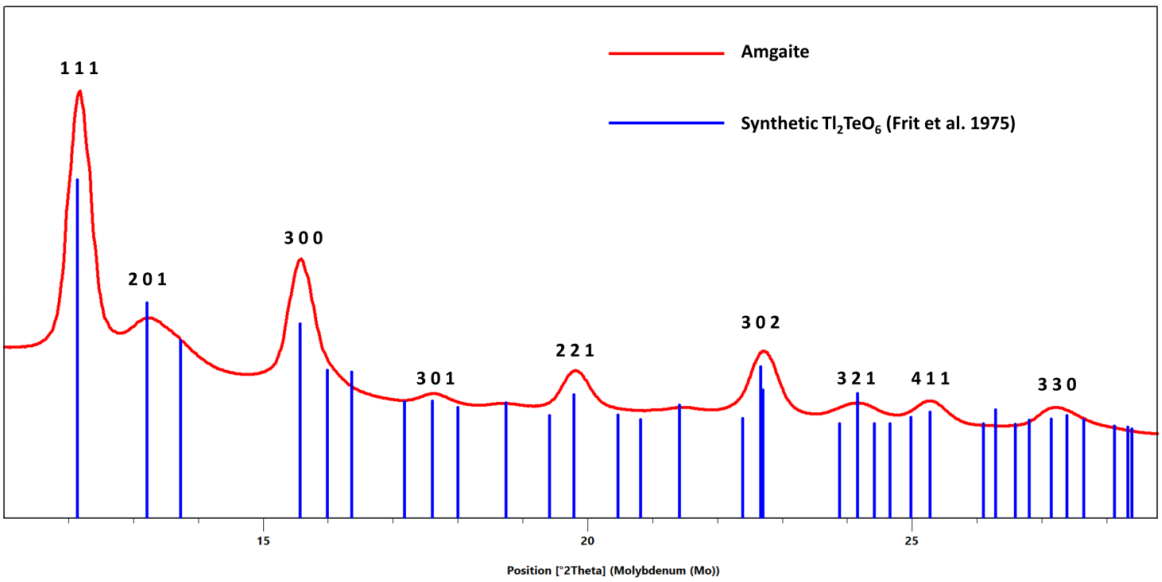

Figure 6. Powder micro-X-ray diffraction pattern for amgaite compared with the lines of synthetic $Tl^{3+}{}_2Te^{6+}O_6$ [20]. The most important diffraction peaks are labeled with their relative Miller indices.

7. Description of Crystal Structure

The crystal structure of amgaite is identical to that of synthetic $Tl^{3+}{}_2Te^{6+}O_6$ [20], as clearly demonstrated by the close match between the PXRD of amgaite and the synthetic phase. Some of the important details of the structure are provided in Table 4.

Table 4. Atomic coordinates and interatomic distances for synthetic $Tl^{3+}{}_2Te^{6+}O_6$ [20].

Atom	x	y	z	B_{iso}
Te1	0.33330	0.66660	0.49875	0.1750
Te2	0.00000	0.00000	0.00000	0.1290
Tl1	0.28558	0.00000	0.50000	0.3580
Tl2	0.62306	0.00000	0.00000	0.3380
O1	0.08770	0.88050	0.77310	1.2400
O2	0.46060	0.59500	0.74170	2.3640
O3	0.21940	0.75750	0.27890	1.1530
		Interatomic distances		
Te1–O1	1.99(3) × 6		Tl1–O1	2.35(3) × 2
			Tl1–O3	2.23(3) × 2
Te2–O2	1.99(4) × 3		Tl1–O2	2.16(5) × 2
Te2–O3	1.95(3) × 3			
			Tl2–O2	2.33(5) × 2
			Tl2–O3	2.26(3) × 2
			Tl2–O1	2.07(3) × 2

The O^{2-} anions constitute a compact, slightly deformed hexagonal stack of which the third and the sixth of the octahedral gaps are occupied by the Tl^{3+} and Te^{6+}, respectively. Figure 7 visualizes the sequence of the occupied octahedra. The two types of octahedra TeO_6 (see Table 4) are regular and almost identical, with six Te–O bonds equal to 1.99 Å for the octahedron $Te1O_6$, three bonds Te–O equal to 1.99 Å and three bonds equal to 1.95 Å for the octahedron $Te2O_6$. On the other side, the TlO_6 octahedra are less regular with

two long, two medium and two short Tl–O distances (see Table 4) and with the mean value in each octahedron Tl1–O_{mean} = 2.24 Å and Tl2–O_{mean} = 2.22 Å. Synthetic $Tl^{3+}{}_2Te^{6+}O_6$ is isostructural to malladrite, Na_2SiF_6 [22]. Each metallic ion is octahedrally coordinated to a slightly distorted anionic hexagonal close-packed array.

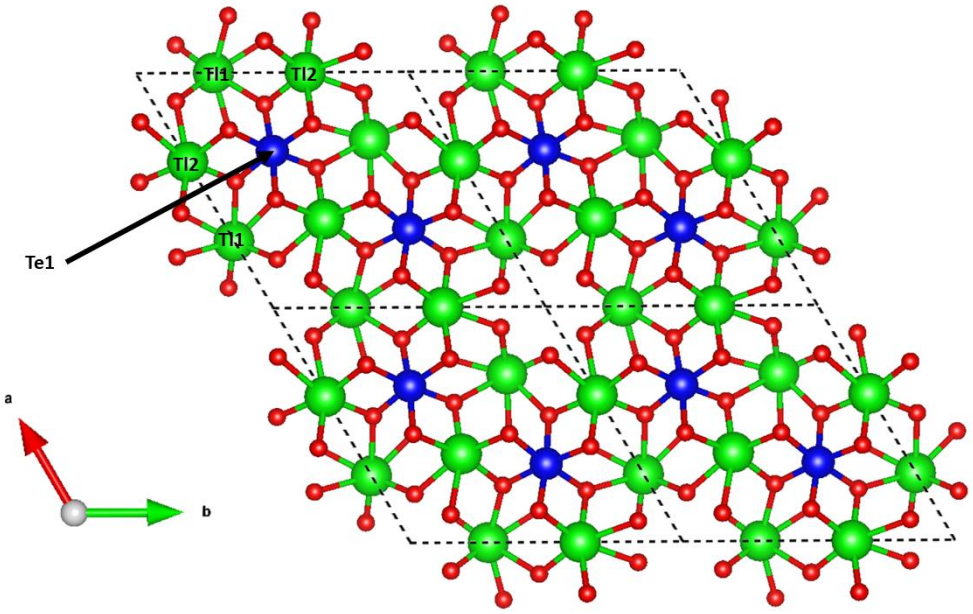

Figure 7. The crystal structure of amgaite along the *c* axis. In blue, the Te sites are shown, while Tl sites are indicated in green (the red spheres correspond to oxygens). The structure data for drawing are from [20]. Tl1 and Tl2 sites are labeled in the figure, as well as the Te1 site. The Te2 site is not visible over such structure orientation, but it runs along the *c* axis. The dashed black lines outline the unit cells.

8. Discussion: Remarks on the Origin and Implications

The friable rocks of the Khokhoyskoe gold deposit where amgaite was found have an obvious supergene origin. They resulted from the oxidation, disintegration, and redeposition in the karst cavities of primary ores such as pyrite-adularia-quartz metasomatites formed during silicic-potassic metasomatism of carbonate rocks. The enrichment of ores by Tl occurred during potassic metasomatism in the fault zones. Very strong oxidative conditions resulted in both Tl and Te reaching their highest valence states in amgaite: +3 and +6, accordingly.

The most updated New IMA List of Minerals includes 85 minerals with species-defining thallium [23]. The overwhelming majority of them contain thallium in its monovalent state, while minerals with trivalent thallium are extremely rare. Amgaite is only the fourth mineral containing Tl^{3+} as a species-defining element after avicennite Tl_2O_3 [24], found at the Khokhoyskoe gold deposit as well [13], and two endemic minerals from the fumaroles of Tolbachik volcano, also known for its extremely oxidative conditions: chrysothallite $K_6Cu_6Tl^{3+}Cl_{17}(OH)_4 \cdot H_2O$ [25] and kalithallite $K_3Tl^{3+}Cl_6 \cdot 2H_2O$ [26]. Tellurates, i.e., minerals with species-defining Te^{6+}, are not that rare (to date, 51 mineral species approved by the IMA CNMNC are known [23]); however, its compounds with Tl were previously unknown in nature. The only other mineral with both Tl and Te, honeaite Au_3TlTe_2 [27,28], is a telluride, i.e., contains Te in anionic form.

The discovery of amgaite along with other Tl minerals such as avicennite, jankovićite, parapierrotite, weissbergite and several as yet unnamed Tl phases [13,15] in the ores of the Khokhoyskoe ore field has an important implication for the industrial gold mining in the region. The unique association of gold with Tl minerals should be considered when choosing a correct technology of gold extraction in view of the high toxicity of thallium, on the one hand, but also its increasing economic value and number of industrial applications

on the other. Since the beginning of the 21st century, thallium has shown a steady upward trend in value–from approximately 1290 USD per kg in 2000 [29] to 8400 USD per kg in 2021 [1]. It is very likely that this trend will remain in the upcoming period as analysts predict the thallium industry to grow at a significant compound annual growth rate and its applications will rise substantially around the globe [30,31]. In this regard, the possible associated extraction of thallium during gold mining gets particular importance.

Author Contributions: Conceptualization, A.V.K. and G.S.A.; Methodology, A.V.K., G.S.A. and F.N., Investigation, A.V.K., G.S.A., F.N., J.P., J.S., R.Š., E.P.S., L.A.K. and V.N.K.; Original Manuscript—Draft Preparation, A.V.K., G.S.A., F.N., J.P., J.S. and R.Š.; Manuscript—Review and Editing, A.V.K., F.N. and J.P.; Figures, A.V.K., G.S.A., F.N. and J.S. All authors have read and agreed to the published version of the manuscript.

Funding: The research was carried out under the governmental project of Diamond and Precious Metal Geology Institute, SB RAS, which was financially supported by the Ministry of Science and Higher Education of the Russian Federation, the project number is 0381-2019-0004. The study was also financially supported by the Ministry of Culture of the Czech Republic (long-term project DKRVO 2019-2023/1.II.d; National Museum, 00023272) for J.S.

Conflicts of Interest: The authors declare no conflict of interest.

References

1. National Minerals Information Center. Available online: https://www.usgs.gov/centers/national-minerals-information-center/thallium-statistics-and-information. (accessed on 6 July 2022).
2. Genchi, G.; Carocci, A.; Lauria, G.; Sinicropi, M.S.; Catalano, A. Thallium use, toxicity, and detoxification therapy: An overview. *Appl. Sci.* **2021**, *11*, 8322. [CrossRef]
3. Jahns, R.H. Clerici solution for the specific gravity determination of small mineral grains. *Am. Miner.* **1939**, *24*, 116.
4. Huifang, X.; Yifeng, W. An equation for predicting binding strengths of metal cations to protein of human serum transferrin. *arXiv* **2017**, arXiv:1711.06724. [q-bio.BM]. [CrossRef]
5. Karbowska, B. Presence of thallium in the environment: Sources of contaminations, distribution and monitoring methods. *Environ. Monit. Assess.* **2016**, *188*, 640. [CrossRef] [PubMed]
6. Manceau, A.; Simionovici, A.; Findling, N.; Glatzel, P.; Detlefs, B.; Wegorzewski, A.; Mizell, K.; Hein, J.; Koschinsky, A. Crystal chemistry of thallium in marine ferromanganese deposits. *ACS Earth Space Chem.* **2022**, *6*, 1269–1285. [CrossRef]
7. Rader, S.T.; Mazdab, F.K.; Barton, M.D. Mineralogical thallium geochemistry and isotope variations from igneous, metamorphic, and metasomatic systems. *Geochim. Cosmochim. Acta* **2018**, *243*, 42–65. [CrossRef]
8. Kasatkin, A.V.; Stepanov, S.Y.; Tsyganko, M.V.; Škoda, R.; Nestola, F.; Plášil, J.; Makovicky, E.; Agakhanov, A.A.; Palamarchuk, R.S. Mineralogy of the Vorontsovskoe gold deposit (Northern Urals). *Mineralogy* **2022**, *8*, 5–93.
9. Kasatkin, A.V.; Plášil, J.; Makovicky, E.; Škoda, R.; Agakhanov, A.A.; Tsyganko, M.V. Pokhodyashinite, $CuTlSb_2(Sb_{1-x}Tl_x)AsS_{7-x}$, a new thallium sulfosalt from the Vorontsovskoe gold deposit, Northern Urals, Russia. *J. Geosci.* **2022**, *67*, 41–51. [CrossRef]
10. Kasatkin, A.V.; Plášil, J.; Makovicky, E.; Chukanov, N.; Škoda, R.; Agakhanov, A.A.; Tsyganko, M.V. Gungerite, $TlAs_5Sb_4S_{13}$, a new thallium sulfosalt with a complex structure containing covalent As-As bonds. *Am. Mineral.* **2022**, *107*, 1164–1173. [CrossRef]
11. Kasatkin, A.V.; Anisimova, G.S.; Nestola, F.; Plášil, J.; Sejkora, J.; Škoda, R.; Sokolov, E.P.; Kondratieva, L.A.; Kardashevskaia, V.N. Amgaite, IMA 2021-104, in: CNMNC Newsletter 66. *Eur. J. Mineral.* **2022**, *34*, 253–257. [CrossRef]
12. Anisimova, G.S.; Kondratieva, L.A.; Kardashevskaia, V.N. Characteristics of supergene gold of Karst cavities of the Khokhoy Gold Ore Field (Aldan Shield, East Russia). *Minerals* **2020**, *10*, 139. [CrossRef]
13. Anisimova, G.S.; Kondratieva, L.A.; Kardashevskaya, V.N. Weissbergite ($TlSbS_2$) and avicennite (Tl_2O_3)—rare thallium minerals. The first finds in Yakutia. *Zap. Ross. Miner. Obs.* **2021**, *2*, 18–27.
14. Anisimova, G.S.; Kondratieva, L.A.; Sokolov, E.P.; Kardashevskaya, V.N. Gold mineralization of the Lebedinsky and Kuranakh types in the Verkhneamginsky district (South Yakutia). *Otechestvennaya Geol.* **2018**, *5*, 3–13.
15. Kondratieva, L.; Anisimova, G. Minerals of Hg, Tl and As of Khokhoy deposit (Aldan shield). In Proceedings of the Geology and Mineral Resources of the North-East of Russia: Materials of the XII All-Russian Scientific and Practical Conference Dedicated to the 65th Anniversary of the Institute of Geology of Diamond and Precious Metals, Siberian Branch of the Russian Academy of Sciences, Yakutsk, Russia, 23–25 March 2022; pp. 184–188. (In Russian)
16. Haeuseler, H. Infrared and Raman spectra and normal coordinate calculations on trirutile-type compounds. *Spectrochim. Acta A Mol. Biomol. Spectrosc.* **1981**, *37*, 487–495. [CrossRef]
17. Blasse, G.; Hordijk, W. The vibrational spectrum of Ni_3TeO_6 and Mg_3TeO_6. *J. Solid State Chem.* **1972**, *5*, 395–397. [CrossRef]
18. Kampf, A.R.; Housley, R.M.; Marty, J. Dagenaisite, a new zinc tellurate from the gold chain mine, Tintic, Utah, USA. *Can. Mineral.* **2017**, *55*, 867–873. [CrossRef]

19. Lafuente, B.; Doens, R.T.; Yang, H.; Stone, N. The power of databases: The RRUFF project. In *Highlights in Mineralogical Crystallography*; Armbruster, T., Danisi, R.M., Eds.; Walter De Gruyter: Berlin, Germany, 2015; pp. 1–30.
20. Frit, B.; Pressigout, R.; Mercurio, D. Synthese et étude structurale du tellurate (VI) de thallium (III) Tl_2TeO_6. *Mater. Res. Bull.* **1975**, *10*, 1305–1312. [CrossRef]
21. Holland, T.J.B.; Redfern, S.A.T. Unit cell refinement from powder diffraction data: The use of regression diagnostics. *Miner. Mag.* **1997**, *61*, 65–77. [CrossRef]
22. Zalkin, A.; Forrester, J.D.; Templeton, D.H. The crystal structure of sodium fluorosilicate. *Acta Cryst.* **1964**, *17*, 1408–1412. [CrossRef]
23. Commission On New Minerals, Nomenclature And Classification. Available online: http://cnmnc.main.jp/ (accessed on 1 August 2022).
24. Karpova, K.N.; Kon'kova, E.A.; Larkin, E.D.; Savel'ev, V.F. Avicennite, a new mineral. *Dokl. Akad. Nauk UzSSR* **1958**, *2*, 23–26. (In Russian)
25. Pekov, I.V.; Zubkova, N.V.; Belakovskiy, D.I.; Yapaskurt, V.O.; Vigasina, M.F.; Lykova, I.S.; Sidorov, E.G.; Pushcharovsky, D.Y. Chrysothallite $K_6Cu_6Tl^{3+}Cl_{17}(OH)_4{\cdot}H_2O$, a new mineral species from the Tolbachik volcano, Kamchatka, Russia. *Miner. Mag.* **2015**, *79*, 365–376. [CrossRef]
26. Pekov, I.V.; Krzhizhanovskaya, M.G.; Yapaskurt, V.O.; Belakovskiy, D.I.; Sidorov, E.G. Kalithallite, IMA 2017-044. CNMNC Newsletter No. 39, October 2017, page 1280. *Miner. Mag.* **2017**, *81*, 1279–1286.
27. Rice, C.M.; Welch, M.D.; Still, J.W.; Criddle, A.J.; Stanley, C.J. Honeaite, a new gold-thallium-telluride from the Eastern Goldfields, Yilgarn Craton, Western Australia. *Eur. J. Miner.* **2016**, *28*, 979–990. [CrossRef]
28. Welch, M.D.; Still, J.W.; Rice, C.M.; Stanley, C.J. A new telluride topology: The crystal structure of honeaite Au_3TlTe_2. *Miner. Mag.* **2017**, *81*, 611–618. [CrossRef]
29. Guberman, D.E. Thallium. In U.S. Geological Survey, 2013, Metal Prices in the United States through 2010: U.S. Geological Survey Scientific Investigations Report 2012–5188. 2013; pp. 178–180. Available online: https://pubs.usgs.gov/sir/2012/5188/sir2012-5188.pdf (accessed on 1 August 2022).
30. *Thallium Market: An Exclusive Study on Upcoming Trends and Growth Opportunities from 2022–2028*; Technical Report; MarketWatch: New York, NY, USA, 2022; Available online: https://www.marketwatch.com/press-release/thallium-market-an-exclusive-study-on-upcoming-trends-and-growth-opportunities-from-2022-2028-2022-08-15 (accessed on 1 August 2022).
31. Global Thallium Market Size 2022 Global Research, Growth Statistics, Business Strategy, Industry Share, Supply-Demand, In-depth Insights by Top Manufacturers, Regional Forecast 2028. Available online: https://southeast.newschannelnebraska.com/story/45954383/global-thallium-market-size-2022-global-research-growth-statistics-business-strategy-industry-share-supply-demand-in-depth-insights-by-top (accessed on 1 August 2022).